ACS ES&T Engineering

pubs.acs.org/estengg

Article

In Vivo Evaluation of Oxygenic Photogranules' Photosynthetic Capacity by Pulse Amplitude Modulation and Phototrophic–Irradiance Curves

Joseph G. Gikonyo,* Andrew Keyser, John Tobiason, Jeeyon Jeong, and Chul Park

Cite This: *ACS EST Engg.* 2021, 1, 551–561

Read Online

ACCESS | Metrics & More | Article Recommendations

ABSTRACT: The commingled microbial moiety of oxygenic photogranules (OPGs) facilitates aeration-free wastewater treatment. Embedded in an extracellular polymeric substances (EPS) matrix, microbial producers and consumers of oxygen occupying granular niches exchange substrates among themselves and with the bulk fluid. An assessment of the OPG's phototrophic potential or functional capacity may require combining different photoactivity signals. The photosynthetic capacity was evaluated using photosynthetic oxygen evolution (POE) and chlorophyll fluorescence (rapid light curves, RLC) measurements using OPGs grown at different light intensities.. A maximum oxygen generating capacity for optimal OPGs and reactor conditions was determined to be 284.4 $mg_{O_2}\ g_{VSS}^{-1}\ h^{-1}$ The OPGs exhibited photoelasticity, with higher photosynthetic capacity in high light (HL) compared to that in low light (LL) adapted samples. Saturation irradiances before the onset of photoinhibition for LL and HL samples were 1000 and 1200 $\mu mol\ m^{-2}\ s^{-1}$, respectively using POE signals, and 478 $\mu mol\ m^{-2}\ s^{-1}$ and 611 $\mu mol\ m^{-2}\ s^{-1}$ using RLC signals. Moreover, HL adapted samples had higher nonphotochemical quenching rates which allude to the OPG's photoelastic potential. The correlation coefficients (κ) between POE and RLCs were lower than reported values for pure microbial cultures reflecting the enhanced contribution from different photosynthetic clades with a variety of light-harvesting pigments present in OPGs. In an OPG reactor, the photochemical activity can be influenced by the granular size, granular ecology, and reactor operation metrics related to irradiance interactions such as mixing, self-shading, light intensity, photoperiods, and reactor depth. This presents opportunities for design of intensive wastewater resource recovery using phototrophic granular biomass.

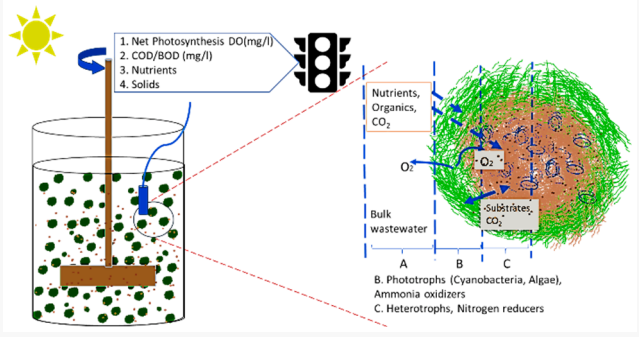

KEYWORDS: *photochemical capacity, oxygenic photogranules, pulse amplitude modulation (PAM), phototrophic irradiance curves, wastewater treatment*

INTRODUCTION

Light energy powers the bulk of primary production in the biosphere with phototrophs transforming this energy into chemical energy[1] for utility at different trophic levels. This light energy is harvested by a moiety of light-harvesting complexes (LHCs) comprising photoreceptors and associated protein complexes.[2] These tetrapyrrole receptors include chlorophyll and phycobilisomes pigments with the latter only present in cyanobacteria[3,4] and chlorophylls in all phototrophs.[2,3,5] The absorbed energy is transferred to reaction centers (II) and (I) protein complexes through a specialized chain of intermediary biomolecules and redox reactions to power carbon assimilation in the Calvin-Benson cycle.[1] Phototrophic autotrophs have developed adaptations to variability in light quantity and quality[6−8] in their environmental niches, such as leaf angles in higher plants and buoyancy regulation in algae and cyanobacteria[9−11] optimizing their photointeraction.

For emerging granular based wastewater systems, such as oxygenic photogranules (OPGs), a consortium of microbes coexists in different associations within the granular ecosystem.[12−14] These biospheres are microreactors exchanging substrates within their matrix[14,15] and beyond their structural boundary with the bulk fluid.[14] This exchange is a function of granular physical properties such as porosity and

Received: November 17, 2020
Revised: January 16, 2021
Accepted: February 9, 2021
Published: February 19, 2021

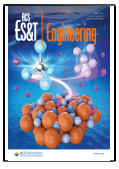

permeability affecting advective, dispersive and diffusive mass transfer.[16,17] These granular properties are in turn a result of the microbial composition, their spatial distribution in the granule morphology[18] and interactions with environmental stresses.[19]

Oxygenic photogranules (OPGs) have a phototrophic outer layer[18,20] enhancing photointeraction. For phototrophs in this layer, an oxygen-evolving complex in the photosystem II (PSII) undertakes photooxidation of water via the KOKs cycle[21,22] producing oxygen. This self-aeration property can be exploited to reduce the high energy demand and cost associated with conventional wastewater treatment.[12,14,18,23] The dissolved oxygen can diffuse into the bulk fluid outside the granular boundary or into the granular core where aerobic oxidation of ammonia and organics by nitrifying bacteria and heterotrophic bacteria, respectively, proliferating in the aerobic zone[18,24] occurs. Concurrently, CO_2 from the oxidation of organics is also available for phototrophic utility. Mature OPGs with diameters >3 mm have anaerobic or anoxic conditions within their stratified core.[18] In this zone, denitrification occurs, reducing nitrate to nitrogen gas.[24] Similarly, nutrients and organic substrates with a concentration gradient between the bulk wastewater and granular environment diffuse into the granular matrix.

Current practices for estimating phototrophic activity involve the use of photosynthetic irradiance (P−I) relations and rapid light curves (RLC).[25,26] The P−I curve relates phototrophic activity as oxygen generated or carbon (^{14}C) consumed in the ordinate over an increasing light intensity abscissa.[11,26] RLC, on the other hand, utilizes the fluorescence characteristics of chlorophyll light-harvesting complexes.[27] Incident pulses of amplitude modulated (PAM) light results in oxidation of reduced reaction centers (RC) and quenching of the incident energy.[28] While P−I curves quantify net photosynthesis, RLC indicates the gross photosynthetic activity.[25,29]

The phototrophic production of both microalgal and cyanobacteria cultures has been widely characterized in pure and mixed cultures.[29−34] However, similar characterization in OPGs and other photogranular biomass existing in a commingled moiety with concurrent production and consumption of substrates in wastewater treatment has not been undertaken. In the tightly coupled microbial environment of phototrophic granules, concurrent generation and consumption of carbon and oxygen within the granular matrix may impede accurate quantification using P−I curves. Moreover, other inherent limitations of the P−I approach include their low sensitivity to low O_2 concentrations and differential uptake of $^{14}C/^{12}C$.[35] On the other hand, phototrophic clades present in OPGs have different accessory light-harvesting pigments such as phycobilins in cyanobacteria which interfere with fluorescence emission while generating RLCs.[29]

In the present work, we explore the photochemical potential of OPGs applied in wastewater treatment using both the P−I curve approach and RLC methods. The P−I approach was modified by utilizing bulk substrate transformations in estimating photosynthetic oxygen production. This characterization will indicate peak oxygen generation, system capacity, and optimal light demand forestalling light's deleterious effects. These parameters are essential for the design of scaled-up photogranular wastewater resource recovery facilities (WRRF).

MATERIALS AND METHODS

Source of Oxygenic Photogranules (OPGs). A sequencing batch reactor (SBR) operated at a 1-d hydraulic retention time (HRT) and fed with wastewater from a local utility was used as a source of OPGs for experimental work. The reactor was seeded with OPG granules[18,36] and operated for 90 days under 200 ± 22 μmol m^{-2} s^{-1} conditions prior to experimental period. The reactor operation was undertaken with sequential light and dark cycles each 3 h long, feeding at the start of the light cycle and a decanting phase at the start of the dark cycle preceded by a 10 min settling phase. Both the decanting and filling events were each undertaken for 5 min. For experimental purposes, the 8 L SBR was operated under two light intensities, 200 ± 22 μmol m^{-2} s^{-1} (low light) and 460 ± 13 μmol m^{-2} s^{-1} (high light), each for 30 d before sampling. The light was provided using daylight mimicking 9 W LEDs (EcoSmart, daylight- 5000 K) with a luminosity of 840 Lumens. In addition, light microscopy (EVOS FL Color AMEFC-4300) was conducted using bright field and epifluorescence (RFP light cube-532 excitation/590 Emission) to characterize morphology and microbial composition. OPGs which have a characteristic cyanobacterial enrichment have golden-orange fluorescence due to the cyanobacteria's phycobiliproteins.[37]

Sample Analysis. Biomass characterization of total suspended solids (TSS) and volatile suspended solids (VSS) were undertaken using Standard Methods 2540D/E[38] and chlorophyll pigments extraction and quantification using Standard Methods 10200H.[38] The phycobilin extraction protocol outlined by Abouhend et al.[18] was modified by centrifuging samples at 12000 rpm for 20 min during processing. The Bennett and Bogorad equation[39] was used to quantify phycobilins substituting 615 nm with abundant 620 nm peaks.[40−42] Effluent samples were also filtered through both 1.5 and 0.45 μm filters and used for analysis of total chemical oxygen demand (COD) and soluble COD fractions, respectively, using Standard Methods 5220C.[38] The 0.45 μm filtrate was also used for the analysis of soluble fractions of total dissolved nitrogen (TDN) and dissolved organic carbon using a TN/TOC analyzer (TOC-VCPH, Shimadzu, USA). Dissolved organic nitrogen was determined as the sum of inorganic nitrogen species (ammonia, nitrite, and nitrate) from TDN. A Metrohm 850 Professional Ion Chromatograph (IC) (Metrohm, Switzerland) was used to measure phosphate and dissolved inorganic nitrogen species.

Photosynthetic Oxygen Evolution (POE). In constructing P−I (hereafter referred to as POE) curves, granules of 0.5 mm to 1 mm in diameter were collected from the reactor by sieve analysis. This size class has been reported as being the most abundant and as having the highest oxygen productivity in OPG reactors.[18] The size sorted granules were then suspended in deionized water (DI) and dark-adapted for 12 h to reduce the reaction centers of photosystems in the light harvesting complexes.[27] In a darkened room, a 1 L glass reactor was then inoculated with the dark-adapted granules and primary effluent wastewater from the local utility prefiltered through 1.5 μm filters. An airtight rubber seal was then used to cap the reactor jar to limit atmospheric interaction. A multiparameter probe (Hanna Instruments) matted to this capping seal and calibrated before every test was then used to record dissolved oxygen, temperature, and pH data at 1 min intervals. A 3 mm diameter tubing drilled into the rubber cap was used as a sampling port. A magnetic stirrer bar calibrated

https://dx.doi.org/10.1021/acsestengg.0c00221
ACS EST Engg. 2021, 1, 551−561

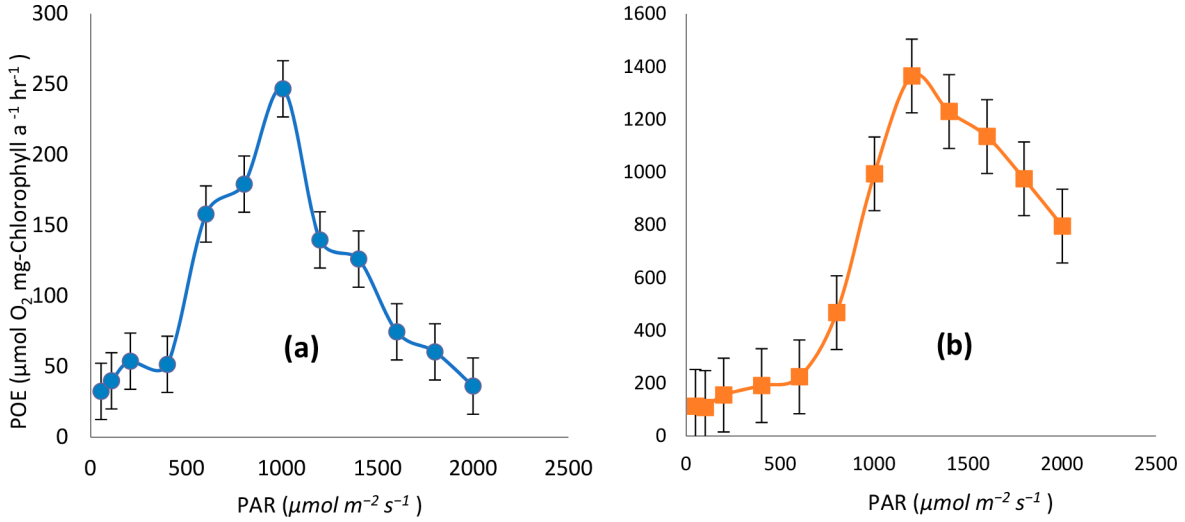

Figure 1. POE determination for OPGs grown at (a) 200 (low light) and (b) 460 μmol m^{-2} s^{-1} (high light) with increasing light intensity. Error bars are standard errors of derived oxygen evolution rates for duplicate reactors with average initial biomass concentrations of 1020 and 1210 mg L^{-1}, respectively. Note different scale used for y axis in these figures.

at 100 rpm was used to provide continuous mixing, while a heat sink was used to maintain the reactor temperature between 22 and 24 °C.

Light was provided at increasing intensities from 50 μmol m^{-2} s^{-1} to 2000 μmol m^{-2} s^{-1} (±10) using an LED panel (6500 K) and calibrated using a Li-Cor 193S underwater spherical sensor (LI-COR Biosciences) at the surface of the reactor. Bulk samples were collected at time 0 and subsequently at two 15 min intervals for every light intensity. In the intervening period between light intensities, the reactor was stored in a darkened enclosure for an average of 8 min. Wastewater was added to suppress dissolved oxygen (DO) saturation in the reactor bulk fluid and to prevent gas loss into the headspace. Net POE was determined as the sum of differential changes in DO concentration, gross nitrification,[43] and COD removal. An oxygen consumption rate of 4.57 $mgO_2/mgNH_3$–N for the oxidation of ammonia[43−45] and a ratio of 1 mgO_2/mgCOD was used for biological oxidation of dissolved organics.

Fluorescence Analysis. Dark-adapted (12 h) granule samples were also analyzed using an imaging pulse amplitude modulation (PAM) fluorometer (M-Series Maxi Version, Walz GmbH, Effeltrich, Germany). Analysis of average light induction (Kautsky effect)[25] was followed by RLC (light-adapted) measurements for granules (n > 30) each delineated as a zone of interest. Samples were collected before and after POE experiments and mounted in DI or wastewater (WW). For light induction measurements, the duration of the light pulses was set to 415 s, with a 40 s interval. Actinic light intensities were set to 186 μmol m^{-2} s^{-1} and 460 μmol m^{-2} s^{-1} for low-light and high-light cultivation conditions, respectively, while the saturating pulses were 5000 μmol m^{-2} s^{-1}. The obtained dark-adapted fluorescence (F_o) and maximal fluorescence (F_m) values were utilized to determine maximal PSII quantum yield[25] as

$$Fv/Fm = (Fm - Fo)/Fm \quad (1)$$

where the variable fluorescence (F_v) is the difference between F_m and F_o.

RLCs characterizing the electron transport rate (ETR) were developed via a stepwise increase of saturating pulses from 0 to 1250 μmol m^{-2} s^{-1}. The effective quantum yield (ϕ_{PSII}) was evaluated over increasing irradiances using light adapted granules[25,29] and was defined as

$$\phi_{PSII} = (Fm' - Fo')/Fm' \quad (2)$$

where F_m' is the light-adapted maximum fluorescence obtained at saturation of reaction centers and F_o' is the light-adapted fluorescence intensity estimated from F_m' measurements.[46] The relative electron transport rate (rETR) was determined as

$$rETR = \phi_{PSII} * PAR \quad (3)$$

which approximates the electron flow in the photosynthetic electron transport chain as a fraction of absorbed quanta to PSII from the ETR determination where PAR is the incident irradiance. Photochemical quenching (qP) which measures the overall reaction center (RC) openness[47] was determined as,

$$qP = (Fm' - F)/(Fm' - Fo') \quad (4)$$

We also evaluated the coefficient of nonphotochemical quenching (qN) describing quenching mechanisms not related to photochemistry.[25]

$$qN = (Fm - Fm')/(Fm - Fo') \quad (5)$$

A Stern−Volmer coefficient of nonphotochemical quenching (NPQ) which is independent of Fo' and has a higher sensitivity to energy quenching within the antennae matrix[11,25] was also determined.

$$NPQ = (Fm - Fm')/(Fm') \quad (6)$$

Curve Fitting. Characteristic photosynthetic parameters were determined by fitting the RLC data with a curve. The Platt empirical estimation (eq 7)[48] describing photosynthesis as a single continuous function of incident light was used.[25] The function covers both the initial increasing photosynthetic rates and the diminishing rate due to irradiance-driven photoinhibition.[49,50] rETR data was exported into origin Pro (v.2020) and processed using the nonlinear curve fit function. A double decay exponential function was fitted onto the data using an orthogonal distance regression algorithm,

https://dx.doi.org/10.1021/acsestengg.0c00221
ACS EST Engg. 2021, 1, 551−561

Table 1. Summary of Photosynthetic Parameters from Chlorophyll Fluorescence Experiments[a]

		POE		RLC			
		200 ± 22	460 ± 13	186		460	
	actinic light (μmol photons m^{-1} s^{-1})	POE	POE	pre-POE	post-POE	pre-POE	
(a)	P_s	4.95×10^{04}	2.03×10^{05}	6.81×10^{03}	3.58×10^{04}	1.26×10^{02}	1.11×10^{04}
	std. error	3.34×10^{08}	4.59×10^{08}	2.97×10^{06}	5.14×10^{06}	3.35×10^{01}	2.51×10^{06}
(b)	alpha (α)	0.78	1.59	0.38	0.37	0.35	0.29
	std. error	0.55	0.78	0.02	0.02	0.02	0.01
(c)	beta (β)	72.5	112.8	17.1	64.2	0.08	17.3
	std. error	4.91×10^{05}	2.58×10^{05}	7.53×10^{03}	9.23×10^{03}	4.90×10^{-02}	3.94×10^{03}
(d)	rETRmax	196	1044	55	76	70	69
(e)	E_k (μmol m^{-1} s^{-1})	250	656	145	205	196	235

[a]The curvilinear double decay function defined in eq 7 was used to estimate growth (α) and decay (β) coefficients, which were then used to compute maximum rETR and E_K. Model parameters are shown in rows a−e with standard errors where included.

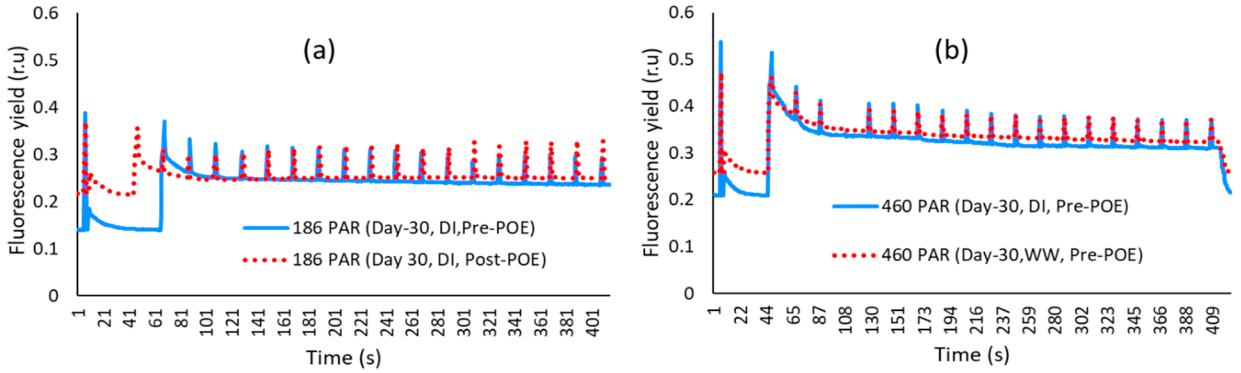

Figure 2. Fluorescence signal plots during light induction (Kautsky effect). (a) OPG biomass grown at 200 μmol m^{-2} s^{-1} with plots taken before (solid) and after (dashed) photosynthetic oxygen evolution (POE) experiments mounted in deionized water (DI). (b) OPG biomass grown at 460 μmol m^{-2} s^{-1} (pre-POE) mounted in DI (solid) and wastewater (WW) (dashed) before oxygen evolution experiments. The vertical axis shows the fluorescence units (arbitrary) with initial maxima and subsequent fluorescence peaks (F') with each saturating pulse. The horizontal axis is in seconds. Representative curves for >60 independent measurements and each peak represents a saturating pulse (5000 μmol m^{-2} s^{-1}) while actinic light (adapted irradiance) is provided at the intervals. The initial peak (F_m) is the maximal fluorescence yield for dark-adapted biomass. PAM fluorescence measurements for low light (200 μmol m^{-2} s^{-1}) cultivation were undertaken at instrument setting equivalent within the range of growth intensity of 186 μmol m^{-2} s^{-1}.

$$P = P_s(1 - e^{-(\alpha E_d/Ps)})e^{-(\beta E_d/Ps)} \quad (7)$$

where P is the photosynthetic rate with E_d (μmol m^{-2} s^{-1}) incident radiation, P_s is the light-saturated rETR without photoinhibition, α is the initial slope of the RLC before saturation, and β characterizes the slope of the RLC during photoinhibition. Additionally, the relative maximum electron transport rate ($rETR_{max}$) and minimum saturating irradiance (E_k) were obtained using the equations described by Ralph et al.[25] The regression analysis was run over 100 iterations to convergence. A coefficient (κ) was determined relating the ETR and POE linear regression in the light-limited region.[11]

RESULTS AND DISCUSSION

Photosynthetic Oxygen Evolution (POE) Characterization. The mean TSS values during POE evaluations were 1288 mg L^{-1} and 1259 mg L^{-1} using low light and high light adapted granule, respectively. VSS/TSS was 0.9 for both sample sets with std.dev 0.01. Mean biomass concentrations evaluated using the t-statistic indicated no statistical difference at P = 0.05. POE curves for both OPG growth irradiances exhibited a typical curvilinear trend with increasing light intensity (Figure 1). Granules cultivated under 460 μmol m^{-2} s^{-1} (high-light condition) showed higher photosynthetic productivity with a peak (1364 μmolO_2 mgChlorophyll a^{-1} hr^{-1}), which was 5.5 times higher than those grown at 200 μmol m^{-2} s^{-1} (low-light condition). Peak photosynthetic activity was observed at 1000 μmol m^{-2} s^{-1} and 1200 μmol m^{-2} s^{-1} for low-light and high-light grown granules, respectively. A regression fit using eq 7 and various photosynthetic parameters are presented in Table 1. The light saturation coefficient (α) in the low-light grown OPGs was 2 times lower than that in high-light OPGs. Moreover, the decay coefficient (β) in the low-light samples was also 1.6 times lower than in the high-light samples while minimum saturation irradiances (E_k) were 250 μmol m^{-2} s^{-1} and 656 μmol m^{-2} s^{-1} for low-light and high-light granules, respectively (Table 1, Figure 1). These higher values for high-light adapted granules allude to photoelasticity of the photosynthetic clades[20] present in OPGs.

Fluorescence Induction in OPGs. The light induction fluorescence yields by OPGs grown under 200 μmol m^{-2} s^{-1} and 460 μmol m^{-2} s^{-1} are presented in Figure 2. Following exposure of the low-light OPGs to high irradiances during POE experiment (up to 2000 μmol m^{-2} s^{-1}), the dark-adapted fluorescence yields (F_o) increased from 0.14 to 0.22 (Figure 2-a). In addition, a 33% decrease in the quantum yield (F_v/F_m) (0.612 → 0.408) ensued from the POE light exposure. These changes allude to high sensitivity of PSII reduction potential in post-POE samples even with dark adaptation, potentially due

https://dx.doi.org/10.1021/acsestengg.0c00221
ACS EST Engg. 2021, 1, 551−561

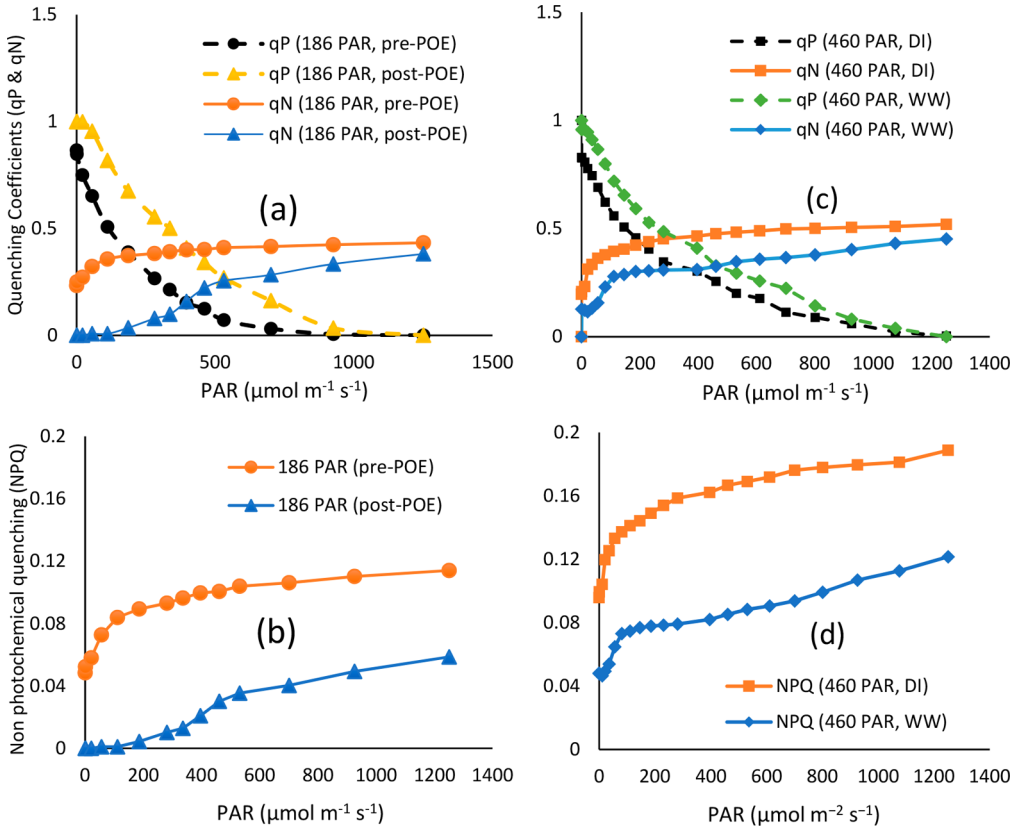

Figure 3. Derived quenching coefficients from RLC applied to light-adapted OPG biomass: photochemical quenching (qP), nonphotochemical quenching (qN), and Stern−Volmer coefficient of nonphotochemical quenching (NPQ) expressed as a function of increasing PAR (μmol m^{-2} s^{-1}). (a) qN and qP for low-light OPGs pre (○) and post (Δ) POE experiments and mounted in DI, (b) NPQ for 200 μmol m^{-2} s^{-1}, (c) qN and qP parameters for 460 μmol m^{-2} s^{-1} (pre-POE) growth irradiance and dark-adapted in DI (□) and WW (◊) and (d) NPQ for 460 μmol m^{-2} s^{-1} growth irradiances. Each representative curve for >60 independent measurements.

to legacy stress, resulting in lower yields.[27] The curves indicate similar trends with relatively constant steady-state fluorescence (F) yields. Moreover, low-light OPGs mounted in DI before and after POE experiments showed comparable maximal fluorescence yields (F_m) of 0.36 and 0.39, respectively (Figure 2-a). The pre-POE samples were dark-adapted for 12 h compared to 4 h for the post-POE samples. Dark-adaptation of phototrophs for long durations can eliminate long-lasting photoinhibition effects (>hours)[25] explaining the similarity in F yields. The similar steady-state yields also suggest that the induced POE irradiance stress was not perpetual.

The pre-POE, high-light granules in DI had a higher F_o(0.21) compared to similarly treated low-light OPGs (Figure 2). In addition, the F_m for these high-light OPGs was also 38% greater than that for low-light OPGs suggesting higher potential capacity of the LHCs compared to low-light OPGs. The quantum yield, F_v/F_m, in high-light OPGs was hence 5% lower than in low-light OPGs. This lowering is a strong indicator of stress conditions on the PSII[27] of high-light OPGs. In comparison to short-term POE irradiance stress on low-light OPGs, high-light OPGs exposed to high irradiances for an extended duration during POE experiments induced persistent stress, seen with higher F levels (Figure 2). The high-light OPGs showed no variability in steady-state fluorescence yields when mounted in WW but had a 20% lower PSII quantum yield than DI-mounted high-light OPGs (Figure 2). Thus, the availability of organic carbon and nutrients in wastewater seems to act a PSII stressor in the high-light OPGs.

Fluorescence Quenching in OPGs. Excess absorbed photon energy is dissipated via photochemical and nonphotochemical pathways characterized by the qP, qN, and NPQ coefficients (Figure 3). The plotted quenching coefficients showed an apparent increase in both qN and NPQ, with a corresponding decrease in qP. For pre-POE, low-light OPGs, the loss in qP capacity diminished to zero at 950 μmol m^{-2} s^{-1}. In contrast, for post-POE, low-light OPGs, the qP diminished to zero at 1200 μmol m^{-2} s^{-1}(Figure 3-a). This alludes to a persistent photochemical capacity with a higher proportion of open PSII reaction centers,[9,27,49] a potential legacy of exposure to high irradiances in post-POE samples. The increase of qP between pre- and post-POE OPGs also suggests an elasticity in the photochemical capacity of the photosynthetic clades in OPGs with growth irradiances.

The heat dissipation coefficients qN and NPQ for the pre-POE low-light granules increased rapidly while those of post-POE samples experienced an initial lag followed by a linear increase (Figure 3-a,b). Linear regression on the initial linear data points resulted in qN slope coefficients of 0.0007 and 0.0005, both showing r^2=0.98, for pre-POE and post-POE samples, respectively (Figure 3-a). Similar fits on the NPQ data resulted in slope coefficients of 0.0003 and 0.00006 (r^2=0.98) (Figure 3-b) equivalent to a rate of 5 times more quenching efficiency for pre-POE biomass. The maximum nonphotochemical quenching potential (NPQ) for pre-POE low-light OPGs was 2 times higher than that of post-POE biomass (Figure 3-a,b). This disparity suggests a higher sensitivity and

https://dx.doi.org/10.1021/acsestengg.0c00221
ACS EST Engg. 2021, 1, 551−561

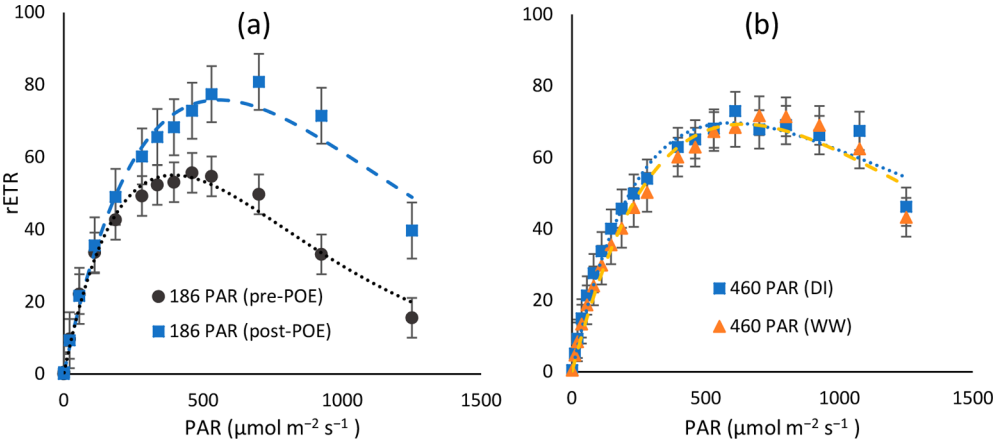

Figure 4. rETR relationship for OPGs grown at different irradiances: (a) low-light OPGs (grown at 200 μmol m^{-2} s^{-1}) and (b) high-light OPGs (grown under 460 μmol m^{-2} s^{-1}). The PAM setting of 8 was used for chlorophyll fluorescence equivalent to 186 μmol m^{-2} s^{-1} actinic light for the low-light cultivation. Dotted lines show the regression fit using the Platt estimation and orthogonal distance regression algorithm and each representative curve for >60 independent measurements.

efficiency of nonphotochemical energy dissipation capacity in the pre-POE samples compared to post-POE samples which had a higher irradiance history.

The differences in induction (Figure 2) and quenching parameters (Figure 3) observed between pre-POE and post-POE low-light OPGs can also be attributed to photochemical recovery kinetics. A component of nonphotochemical quenching associated with photoinhibition (qI)[27,51] has been reported to have slower relaxation >30 min to hours. This slow relaxation is also responsible for energy redistribution to PSII.[25] Quenching related to energy-dependent and state transition occurs over shorter time scales (<30 min).[25,27,49,51,52]

The qP coefficients in high-light adapted OPGs decreased to a minimum at 1251 μmol m^{-2} s^{-1} (Figure 3-c) for OPGs in both DI and WW, comparable to low-light post-POE samples. With WW the qP potential was higher by 0.15 r.u up to 800 μmol m^{-2} s^{-1} as compared to high-light samples in DI. The qN coefficient for OPGs in DI had a steep linear increase up to 0.32 at low PAR at 21 μmol m^{-2} s^{-1}, subsequently lagging to a maximum of 0.52 at 1251 μmol m^{-2} s^{-1}. On the other hand, samples in WW experienced a lower qN capacity with a rapid linear increase to 0.28 at a higher intensity of 111 μmol m^{-2} s^{-1} and a maximum of 0.45 at 1251 μmol m^{-2} s^{-1}. The regression coefficient fit on the linear increase slope was 0.005 for DI mounted samples and 0.002 for WW inoculates (r^2=0.97).

In addition, the NPQ potential for high-light OPGs was higher in DI than WW with a maximum of 0.19 and 0.12, respectively (Figure 3-d). Regression fit on the linearly increasing NPQ data points resulted in slope coefficients of 0.001 for DI and 0.0003 for WW mounted samples (r^2=0.97), indicating a 3.3 times higher NPQ efficiency for high-light OPGs mounted in DI. Despite the similarity of steady-state fluorescence (F) yields (Figure 3-b), inoculating HL OPGs in WW confers some photochemical quenching resilience compared to DI. This can be attributed to amendment of photosynthetic activity by substrates in WW. NPQ for DI mounted samples was also higher in high-light OPGs compared to low-light OPGs and similar to observed fluorescence yield trends, indicating a higher heat loss rate constant.

The high-light OPGs had higher photosynthetic quenching (qP) capacity than low-light OPG biomass (Figure 3). Similarly, low-light OPGs exposed to high light intensities during POE experiments exhibited similar qP trend and saturating intensity (1251 μmol m^{-2} s^{-1}) to high-light OPGs. These results indicate the inherent elasticity of photochemical moiety in the OPG biomass. Both the low-light and high-light OPGs mounted in DI exhibited a similar trend of nonphotochemical quenching (qN and NPQ) potential, but high-light OPGs had higher peaks (Figure 3). The initial rate of qN increase was also 2.9 times higher for high-light OPGs in DI than comparable low-light OPG conditions. This nonphotochemical quenching trend again suggests that OPG growth at higher irradiances results in more rapid responses to inhibiting light.

Photochemical Efficiency in OPGs. The product of effective quantum yield (ϕ_{PSII}) and PAR gives a relative indication of actual electron transport efficiency[25,27] since the ϕ_{PSII} is independent of light-harvesting pigment concentrations. The plots of rETR and irradiance exhibited a curvilinear relationship (Figure 4) characterized by monotonic increase, a light-limited butte with maximum rETR and an electron transport limited decrease. Low-light OPGs experienced a 1.4 times increase in rETR peak (from 55 to 75.8) by exposure to higher light during POE experiments (Figure 4-a). Pre-POE OPGs cultivated under high-light conditions had comparable $rETR_{max}$ of 69.6 and 69.3 when inoculated in DI and WW, respectively, attained at irradiance of 611 μmol m^{-2} s^{-1} (Figure 4-b).

The model fit on the RLC and POE data revealed the light saturation coefficient (α) for both low-light and high-light samples at 0.35 ± 0.04 under all conditions (Table 1-b). This result alludes to comparable photosynthetic clades and response for the OPGs analyzed, in light-limited conditions. In contrast, the decay coefficient (β) for pre-POE low-light OPGs was 17.1, 3.8 times lower than that of post-POE samples. This RLC decay coefficient for post-POE samples (64.2) was comparable to values obtained from the POE model of low-light samples (72.5) (Table 1). In high-light samples, a lower β was obtained for DI mounted samples (0.08) compared to WW mounted samples (17.3), indicating a lower sensitivity to saturating light conditions. The higher

https://dx.doi.org/10.1021/acsestengg.0c00221
ACS EST Engg. 2021, 1, 551−561

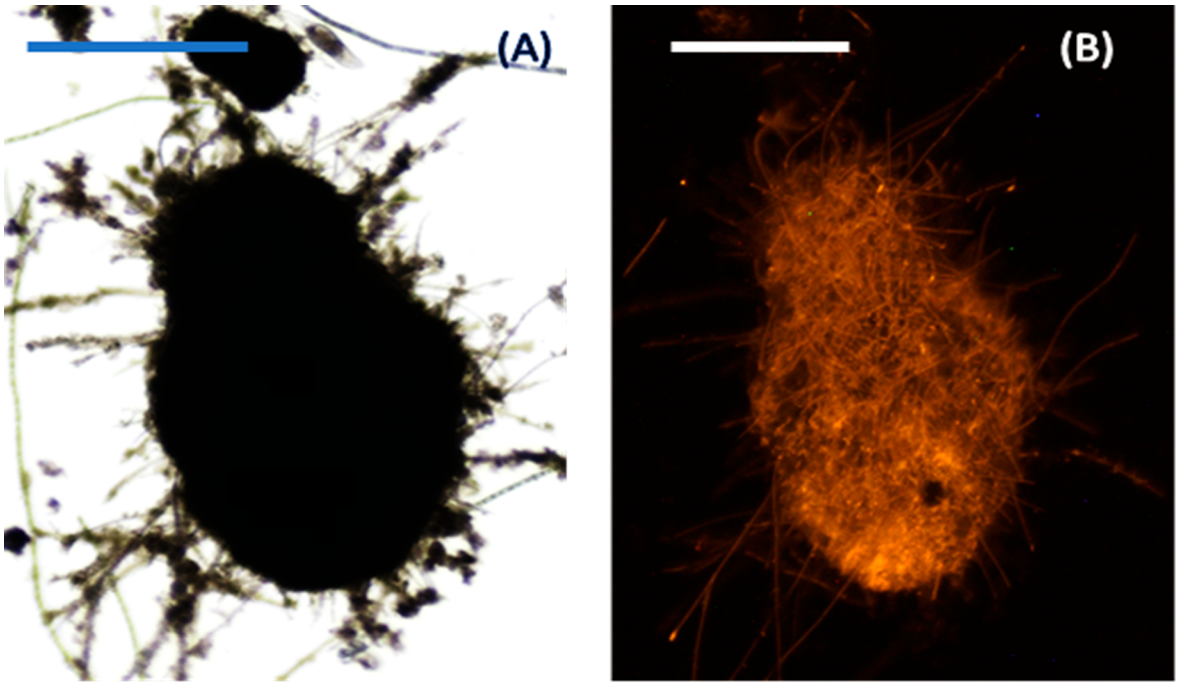

Figure 5. Microscopic images of oxygenic photogranule (OPGs) from reactor used in photochemical evaluation. (A) Brightfield light microscopy (scale bar 500 μm). (B) Phycobilin autofluorescence of filamentous cyanobacteria within the photogranule shown in panel A (scale bar is 500 μm).

decay rate could be reflective of elevated microbial activity in WW compared to DI.

A lower minimum saturating irradiance (Ek) was obtained for pre-POE low-light OPG samples, 145 μmol m^{-2} s^{-1}, as compared to 205 μmol m^{-2} s^{-1} for post-POE samples (Table 1). This result parallels the higher qP values in post-POE samples (Figure 3) suggesting plasticity of OPG photosynthetic clades. A higher proportion of PSII centers remain open[27] at higher irradiances even with short-term adaptation to higher light intensity. The difference in pre- and post-POE minimum saturating irradiances could also be imputed to either design differences of RLC and POE experiments and or OPG morphology.[15,18] The Ek for high-light samples (pre-POE) were 196 μmol m^{-2} s^{-1} and 235 μmol m^{-2} s^{-1} when mounted in DI and WW, respectively (Table 1). These irradiances were lower than those determined from POE experiments with high-light OPGs (656 μmol m^{-2} s^{-1}) (Table 1). The efficiency relation parameter (κ)[53] was significantly higher (P = 0.05) for high-light OPGs (1.8) compared to low-light OPGs (0.7) with a linear relationship observed (Figure 5). A narrow range of this relation has been reported for green algae (1.9−4.9) compared to that of cyanobacteria (2.9−9.2) and diatoms (0.6−6.4),[11] which are all present in OPGs.[15,20,54]

Light intensity within the photochemical range of the granular biomass fosters optimal production and consumption of oxygen. The maximum rETR (196) for POE experiments at the saturating rate was 5.3 times lower in low-light than high-light OPGs with a corresponding saturating irradiances (E_k) ratio of 2.6 (Table 1). This represents a doubling of the rETR with increase in POE saturating irradiance. In addition, the saturation rate coefficient (α) increased 2-fold for POE experiments (Table 1) equivalent to the ratio growth irradiances. One theory to explain this increase is the higher light penetration into the granular matrix at higher irradiances activating more photoactivity.

In WRRF processes, target dissolved oxygen levels indicate the treatment efficacy.[55] These results therefore suggest that when light is limited, the hydraulic retention times in OPG reactors can be increased to reflect the reduced oxygen generation capacity of the system. High photon energy can, on the other hand, results in photoinhibition.[49] From the POE model fit (Table 1), high-light OPGs had a 1.6 times higher decay coefficient (β) than low-light OPGs. Despite adaptation to higher growth irradiance, which can be learned from higher qP and fluorescence yields compared to low-light OPGs, the higher decay coefficient, qN and NPQ in high-light OPGs indicates a rapid loss of photosynthetic potential.

Comparison between PAM and RLCs. PAM utilizes chlorophyll fluorescence signals to characterize photochemical activity. The RLC derived from fluorescence experiments resulted in lower peak irradiances (Figure 4) compared to POE (Figure 1). Maximum saturation rates (α) from RLC data for low-light OPGs and high-light OPGs were comparable (0.38 and 0.35) for DI mounted samples (Table 1). However, these rates were 2.1 and 5.4 times lower than corresponding POE data, respectively. Similarly, the decay rates were also 4.2 and 6.5 times lower for RLC experiments (Table 1). POE experiments induce steady-state conditions at each light intensity while short light pulses utilized in RLC experiments could account for the lower RLC model coefficients.[25]

Moreover, RLCs are dependent on the light prehistory of the phototrophic moiety while POE curves indicate the optimal conditions independent of light history.[25] As both POE and RLC samples were pretreated similarly, their different coefficient values can also be attributed to the morphology and stratification of the OPGs.[15,18] OPG morphology consists of layered microbial niches with the phototrophic zone at their surface.[18] Internally localized heterotrophs oxidize organic carbon in wastewater generating CO_2 available for photosynthesis. The diffusive transfer of these substrates into and out of the different OPG layers may

https://dx.doi.org/10.1021/acsestengg.0c00221
ACS EST Engg. 2021, 1, 551−561

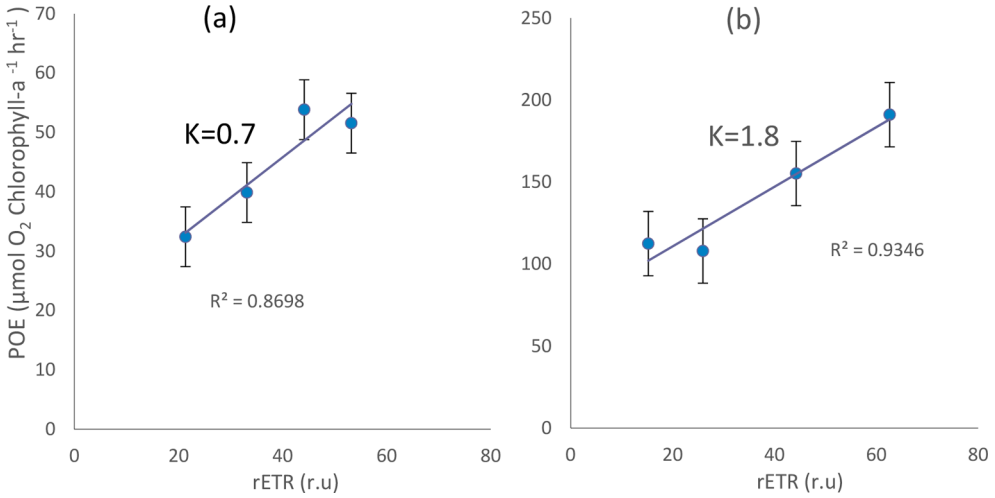

Figure 6. Linear regression fit on the first four data points in the POE light-limited region correlated to equivalent rETR values: (a) low-light OPGs (grown at 200 μmol m^{-2} s^{-1}) and (b) high-light OPGs (grown under 460 μmol m^{-2} s^{-1}). κ relates the photosynthetic electron transport efficiency to photosynthesis efficiency. Error bars are standard errors of derived POE and rETR relation.

occur at temporal magnitudes higher than that of the fluorescence pulses. This contrasts with apparent substrate amendment of photochemical electron sinks in POE evaluation.

Additionally, RLC illumination of the photosynthetic culture is 1-dimensional, similar to that of pure cultures and plants.[11,25,56] The resulting fluorescence and estimations of ETR represent partial light utility in the spheroidal OPG aggregates. In comparison, POE experiments which exhibited higher model coefficients and saturating irradiances reflect overall granule utility. Granular spin resulting from mixing operations and particle−particle interactions in POE determination could expose more photosynthetic apparatus to light (Figure 5). Moreover, variable light penetration in relation to OPG stratification[18] could result in shading and, hence, lower POE activity.[57] This variable interaction can impact light utility within a reactor setting.

The observed differences in POE and RLC parameters (Table 1) can also be attributed to the cyanobacterial population in OPGs.[20] The presence of fluorescent accessory pigments such as phycobilins can compromise interpretation of cyanobacteria fluorescence (Figure 5-b).[29] In addition, cyanobacteria have evolved energy redistribution mechanisms between the photosystems (I and II), eliminating electron transport imbalances.[29] These rapid state transitions present even in the dark can compromise the determination of nonphotochemical quenching (qN).[11] In cyanobacteria, production and consumption pathways intersect in the same thylakoid membranes while also sharing the z-scheme plastoquinone acceptors.[29] At high irradiances, significant electron losses can occur in cyanobacteria with losses of 50−70% of average rates reported in *Synechosystis* sp. PCC 6803.[11]

Additionally, oxygen uptake by respiration, cyclic electron flow around PSII, and Mehler reactions where oxygen becomes reduced forming superoxide radicals occurs in cyanobacteria.[29,49,58] These competing needs can lead to underestimation of the oxygen generation from cyanobacteria,[29] an integral clade in OPGs and seen with different POE and rETR saturation values (Table 1). In addition, nitrogen assimilation can cause lower photon yields (ϕ) of both POE and rETR.[56] Chlorophyll quenching has been reported to consistently understate the efficiency of the photosynthetic production in cyanobacteria. The low values can be attributed to understated yield parameters (F_0 and F_m).[29] Schuurmans et al. hence suggested a qualitative interpretation of RLC data.[29]

The relation of POEand RLC yields characterized by the κ parameter (Figure 6) for low-light OPGs (0.7) and high-light OPGs (1.8) are within the range of literature reported values for pure culture phototrophic microbes.[11] These values reflect a mean activity of the commingled phototrophic consortia in OPGs and are lower than maximum values reported for cyanobacteria (κ = 9.2) but within the lower limit reported for diatoms (κ = 0.6). RLCs result in higher variability of this correlation for cyanobacteria and diatoms[11,29] and hence they are recommended for use qualitatively to describe the state of PSII.[11,29]

Implications on OPGs' Photosynthetic Capacity and Reactor Operation. Typical POE experiments entail strict quantifying of carbon consumption or oxygen evolution from the prototrophic assemblage.[11,25,33] However, this pioneering approach to characterize phototrophic activity in granular structures presents challenges. Specifically, granular stratification and variable distribution of phototrophic biomass within the granules of different sizes[14,18] negate the equivalence of bulk and individual granule photochemical capacities. The OPG size class (0.5−1 mm) utilized for determination of photochemical capacity in this study were reported to be most abundant within an OPG reactor and as having the highest oxygen generation potential (specific oxygen production rate of 21.9 ± 1.3 mg_{O_2} g_{VSS}^{-1} h^{-1}).[18,20,54] This oxygen production rate was also 75% higher than that of the mixed reactor biomass[18,54] and approximates to a POE of 60 μmol_{O_2} $mg_{chlorophyll a}^{-1}$ h^{-1}. This generation is 4 times lower than the determined maximum POE value, 247 μmol_{O_2} $mg_{chlorophyll a}^{-1}$ h^{-1}, of low-light OPGs (Figure 1).

Similarly, we can infer a mixed biomass oxygen production of 141 μmol_{O_2} $mg_{chlorophyll a}^{-1}$ h^{-1} (51.5 mg_{O_2} g_{VSS}^{-1} h^{-1}) from our reported POE data for low-light OPGs. The maximum POE obtained using high-light OPGs of 1364.7 μmol_{O_2} $mg_{chlorophyll a}^{-1}$ h^{-1} equates to a mixed biomass specific oxygen production of 284.4 mg_{O_2} g_{VSS}^{-1} h^{-1}. This ideal capacity is sufficient for treatment of most domestic wastewater streams at

https://dx.doi.org/10.1021/acsestengg.0c00221
ACS EST Engg. 2021, 1, 551−561

modest retention times. However, light interaction limitations in reactors can adversely limit this capacity in addition to photoinhibitory effects where bright sunlight is utilized.[49] The POE data indicates that irradiances above 1200 μmol m^{-2} s^{-1} would generally result in decreased photosynthetic production by OPGs, while full sunlight has about 2000 μmol m^{-2} s^{-1}. Beyond inhibition, long-term exposure to this irradiance would result in photooxidation and cellular mortality[59] of OPG photosynthetic moieties.

High oxygen concentration within the granular matrix can inhibit denitrification[14] while low concentrations can result in reduced COD oxidation and nitrification rates by aerobic microbes within the granule.[23,36,54] Above saturation concentrations of oxygen within granules can induce oxidative stress in cells from reactive oxygen species and competition with CO_2(low CO_2/ O_2) for ribulose-1,5-bisphosphate carboxylase/oxygenase (Rubisco)[60] and, hence, decrease the electron transport rates. Additionally, some oxygen generated within the OPGs dissolves into the bulk fluid. At high light intensities, the photosynthetic rate can be greater than the rate of oxygen consumption hence respiration becomes the rate-limiting process for wastewater treatment. In the design of photobioreactors,[61] maintaining a balance between oxygen consumption and production should, therefore, be considered in the determination of hydraulic retention time.

Moreover, carbon transfers within the granule occur via multiple pathways.[31] Organic carbon is oxidized to CO_2 by heterotrophic oxidation. This carbon product can become available for photosynthetic activity resulting in mutualistic associations.[14] Inorganic carbon from the atmosphere can also be available for phototrophic activity via carboxylation[60,62] in the wastewater stream, a process enhanced by mixing operations. We operated the POE experiments with minimal environmental interaction to limit this external addition of CO_2. Typical carbon tracing for POE construction quantifies photosynthetic targeted inorganic carbon (^{14}C)[25,35] and may not capture organic source derived carbon. Additionally, phototrophic microbes, including cyanobacteria, present in OPGs have versatile carbon assimilation and concentration mechanisms.[27,63] Members of the genus *Oscillatoria* and *Microcoleus* and chlorophytes genera *Scenedesmus*, which are dominant in OPGs,[20,64] have been reported mixotrophic capacity.[65,66] This metabolic diversity enables microbes to survive in light-limited conditions by the synthesis of organic carbon sources. Hence, carbon use within an OPG reactor may be understated due to this uptake in light-limited granule zones affecting POE estimations. This versatility also incurs a metabolic cost that may depress electron transport values for RLC estimations.

In OPG reactors, the optimal photochemical capacity determined via POE experiments and dependent on growth irradiances can be lessened by variable particle flow within the reactor.[67,68] The mixing speed influences the frequency of "OPGs to see light" events[69,70] and longer exposures to supra saturating irradiances generally above 1000−1200 μmol m^{-2} s^{-1} can result in photoinhibition.[49,71,72] Extended periods in the dark facilitate recovery from photoinhibition but can also lead to elevated respiration.[57,73,74] Self-shading effects resulting from particle interaction in relation to the optical path also depend on the size and biomass concentrations (Figure 5).[57] A priori, the bulk-fluid mixing pattern is a function of reactor size, impeller design, and mixing intensity. Moreover, particulate interactions and intragranule substrate transfers depend on their physical permeability and porous characteristics. Availability of substrates for photosynthesis can also impact this optimal photochemical capacity as seen with WW mounted OPGs. These factors can cause deviation from maximal photosynthetic capacity in operation of photogranular WW treatment adding to optimization complexity. Further research and evaluation of these reactor operation matrices is necessary to optimize these systems.

AUTHOR INFORMATION

Corresponding Author

Joseph G. Gikonyo − *Department of Civil and Environmental Engineering, University of Massachusetts, Amherst, Massachusetts 01003, United States;* orcid.org/0000-0001-5035-4059; Email: jgikonyo@umass.edu

Authors

Andrew Keyser − *Department of Civil and Environmental Engineering, University of Massachusetts, Amherst, Massachusetts 01003, United States*

John Tobiason − *Department of Civil and Environmental Engineering, University of Massachusetts, Amherst, Massachusetts 01003, United States;* orcid.org/0000-0002-1313-9955

Jeeyon Jeong − *Department of Biology, Amherst College, Amherst, Massachusetts 01002, United States*

Chul Park − *Department of Civil and Environmental Engineering, University of Massachusetts, Amherst, Massachusetts 01003, United States;* orcid.org/0000-0003-0695-8562

Complete contact information is available at: https://pubs.acs.org/10.1021/acsestengg.0c00221

Notes

The authors declare no competing financial interest.

ACKNOWLEDGMENTS

We thank and acknowledge the contributions of Kaitlyn Tsuyuki (Amherst College) in fluorescence imaging and Arfa Ansari and Andrew Keyser (UMass-Amherst) during experimental analysis. This work was supported by the National Science Foundation [IIP1919091].

REFERENCES

(1) Liu, J.; Lu, Y.; Huia, W.; Last, R. L. A New Light on Photosystem II Maintenance in Oxygenic Photosynthesis. *Front. Plant Sci.* **2019**, DOI: 10.3389/fpls.2019.00975.

(2) Green, B.; Parson, W. W. *Light-Harvesting Antennas in Photosynthesis*, 1st ed.; Springer Science & Business Media, 2003; Vol. *13*.

(3) Saer, R. G.; Blankenship, R. E. Light Harvesting in Phototrophic Bacteria: Structure and Function. *Biochem. J.* **2017**, *474* (13), 2107−2131.

(4) Singh, N. K.; Sonani, R. R.; Rastogi, R. P.; Madamwar, D. The Phycobilisomes: An Early Requisite for Efficient Photosynthesis in Cyanobacteria. *EXCLI J.* **2015**, *14*, 268−289.

(5) Young, A. J. Occurrence and Distribution of Carotenoids in Photosynthetic Systems. In *Carotenoids in Photosynthesis*; Young, A. J., Britton, G., Eds.; Springer Netherlands: Dordrecht, 1993; pp 16−71. DOI: 10.1007/978-94-011-2124-8_2.

(6) Bernstein, H. C.; Konopka, A.; Melnicki, M. R.; Hill, E. A.; Kucek, L. A.; Zhang, S.; Shen, G.; Bryant, D. A.; Beliaev, A. S. Effect of Mono- and Dichromatic Light Quality on Growth Rates and

Photosynthetic Performance of Synechococcus Sp. PCC 7002. *Front. Microbiol.* **2014**, DOI: 10.3389/fmicb.2014.00488.
(7) Wu, H. Effect of Different Light Qualities on Growth, Pigment Content, Chlorophyll Fluorescence, and Antioxidant Enzyme Activity in the Red Alga Pyropia Haitanensis (Bangiales, Rhodophyta). *BioMed. Res. Int.* **2016**, DOI: 10.1155/2016/7383918.
(8) Zhang, B.; Guo, Y.; Lens, P. N. L.; Zhang, Z.; Shi, W.; Cui, F.; Tay, J. H. Effect of Light Intensity on the Characteristics of Algal-Bacterial Granular Sludge and the Role of N-Acyl-Homoserine Lactone in the Granulation. *Sci. Total Environ.* **2018**, DOI: 10.1016/j.scitotenv.2018.12.250.
(9) Bailey, S.; Grossman, A. Photoprotection in Cyanobacteria: Regulation of Light Harvesting. *Photochem. Photobiol.* **2008**, *84* (6), 1410−1420.
(10) Berg, M.; Sutula, M. *Factors Affecting the Growth of Cyanobacteria with Special Emphasis on the Sacramento—San Joaquin Delta*, Technical Report 869; Southern California Coastal Water Research Project, August 2015.
(11) Masojidek, J. Photosystem II Electron Transport Rates and Oxygen Production in Natural Waterblooms of Freshwater Cyanobacteria During a Diel Cycle. *J. Plankton Res.* **2001**, *23* (1), 57−66.
(12) Milferstedt, K.; Hamelin, J.; Park, C.; Jung, J.; Hwang, Y.; Cho, S.-K.; Jung, K.-W.; Kim, D.-H. Biogranules Applied in Environmental Engineering. *Int. J. Hydrogen Energy* **2017**, *42* (45), 27801−27811.
(13) Liu, L.; Fan, H.; Liu, Y.; Liu, C.; Huang, X. Development of Algae-Bacteria Granular Consortia in Photo-Sequencing Batch Reactor. *Bioresour. Technol.* **2017**, *232*, 64−71.
(14) Lee, Y.-J.; Lei, Z. Microalgal-Bacterial Aggregates for Wastewater Treatment: A Mini-Review. *Bioresour. Technol. Rep.* **2019**, *8*, 100199.
(15) Kuo-Dahab, W. C.; Stauch-White, K.; Butler, C. S.; Gikonyo, G. J.; Carbajal-González, B.; Ivanova, A.; Dolan, S.; Park, C. Investigation of the Fate and Dynamics of Extracellular Polymeric Substances (EPS) during Sludge-Based Photogranulation under Hydrostatic Conditions. *Environ. Sci. Technol.* **2018**, *52* (18), 10462−10471.
(16) Li, D.; Ganczarczyk, J. Advective Transport in Activated Sludge Flocs. *Water Environ. Res.* **1992**, *64* (3), 236−240.
(17) Sears, K.; Alleman, J. E.; Barnard, J. L.; Oleszkiewicz, J. A. Density and Activity Characterization of Activated Sludge Flocs. *J. Environ. Eng.* **2006**, *132* (10), 1235−1242.
(18) Abouhend, A. S.; Milferstedt, K.; Hamelin, J.; Ansari, A. A.; Butler, C.; Carbajal-González, B. I.; Park, C. Growth Progression of Oxygenic Photogranules and Its Impact on Bioactivity for Aeration-Free Wastewater Treatment. *Environ. Sci. Technol.* **2019**, *54* (1), 486−496.
(19) Bindhu, B. k.; Madhu, G. Selection Pressure Theory for Aerobic Granulation - an Overview. *Int. J. Environ. Waste Manage.* **2014**, *13* (3), 317−329.
(20) Milferstedt, K.; Kuo-Dahab, W. C.; Butler, C. S.; Hamelin, J.; Abouhend, A. S.; Stauch-White, K.; McNair, A.; Watt, C.; Carbajal-González, B. I.; Dolan, S.; Park, C. The Importance of Filamentous Cyanobacteria in the Development of Oxygenic Photogranules. *Sci. Rep.* **2017**, *7* (1), 17944.
(21) Brudvig, G. W. Water Oxidation Chemistry of Photosystem II. *Philos. Trans. R. Soc., B* **2008**, *363* (1494), 1211−1219.
(22) Najafpour, M. M.; Govindjee. Oxygen Evolving Complex in Photosystem II: Better than Excellent. *Dalton Trans.* **2011**, *40*, 9076.
(23) Park, C.; Dolan, S. Algal-Sludge Granule for Wastewater Treatment and Bioenergy Feedstock Generation. US 10189732 B2, January 29, 2019.
(24) Giesen, A.; van Loosdrecht, M.; Pronk, M.; Robertson, S.; Thompson, A. Aerobic Granular Biomass Technology: Recent Performance Data, Lessons Learnt and Retrofitting Conventional Treatment Infrastructure. *Proc. Water Environ. Fed.* **2016**, No. 11, 1913−1923.
(25) Ralph, P. J.; Gademann, R. Rapid Light Curves: A Powerful Tool to Assess Photosynthetic Activity. *Aquat. Bot.* **2005**, *82* (3), 222−237.
(26) MacIntyre, H. L.; Kana, T. M.; Anning, T.; Geider, R. J. Photoacclimation of photosynthesis irradiance response curves and photosynthetic pigments in microalgae and cyanobacteria1. *J. Phycol.* **2002**, *38* (1), 17−38.
(27) Murchie, E. H.; Lawson, T. Chlorophyll Fluorescence Analysis: A Guide to Good Practice and Understanding Some New Applications. *J. Exp. Bot.* **2013**, *64* (13), 3983−3998.
(28) *Chlorophyll a Fluorescence in Aquatic Sciences: Methods and Applications*; Suggett, D. J., Prášil, O., Borowitzka, M. A., Eds.; Springer Netherlands: Dordrecht, 2010. DOI: 10.1007/978-90-481-9268-7.
(29) Schuurmans, R. M.; van Alphen, P.; Schuurmans, J. M.; Matthijs, H. C. P.; Hellingwerf, K. J. Comparison of the Photosynthetic Yield of Cyanobacteria and Green Algae: Different Methods Give Different Answers. *PLoS One* **2015**, *10* (9), No. e0139061.
(30) Campbell, D.; Hurry, V.; Clarke, A. K.; Gustafsson, P.; Öquist, G. Chlorophyll Fluorescence Analysis of Cyanobacterial Photosynthesis and Acclimation. *Microbiol. Mol. Biol. Rev.* **1998**, *62* (3), 667−683.
(31) Pastore, M.; Santaeufemia, S.; Bertucco, A.; Sforza, E. Light Intensity Affects the Mixotrophic Carbon Exploitation in Chlorella Protothecoides: Consequences on Microalgae-Bacteria Based Wastewater Treatment. *Water Sci. Technol.* **2018**, *78* (8), 1762−1771.
(32) Malapascua, J.; Jerez, C.; Sergejevová, M.; Figueroa, F.; Masojídek, J. Photosynthesis Monitoring to Optimize Growth of Microalgal Mass Cultures: Application of Chlorophyll Fluorescence Techniques. *Aquat. Biol.* **2014**, *22*, 123−140.
(33) Bouman, H. A.; Platt, T.; Doblin, M.; Figueiras, F. G.; Gudmundsson, K.; Gudmundsson, H. G.; Huang, B.; Hickman, A.; Hiscock, M.; Jackson, T.; Lutz, V. A.; Mélin, F.; Rey, F.; Pepin, P.; Segura, V.; Tilstone, G. H.; van Dongen-Vogels, V.; Sathyendranath, S. Photosynthesis-Irradiance Parameters of Marine Phytoplankton: Synthesis of a Global Data Set. *Earth System Science Data* **2018**, *10*, 251−266, DOI: 10.5194/essd-10-251-2018.
(34) Corcoll, N.; Ricart, M.; Franz, S.; Sans-Piché, F.; Schmitt-Jansen, M.; Guasch, H. The Use of Photosynthetic Fluorescence Parameters from Autotrophic Biofilms for Monitoring the Effect of Chemicals in River Ecosystems. In *Emerging and Priority Pollutants in Rivers*; Guasch, H., Ginebreda, A., Geiszinger, A., Eds.; Springer: Berlin, 2012; Vol. *19*, pp 85−115. DOI: 10.1007/978-3-642-25722-3_4.
(35) Macedo, M.; Ferreira, J.; Duarte, P. Dynamic Behaviour of Photosynthesis-Irradiance Curves Determined from Oxygen Production during Variable Incubation Periods. *Mar. Ecol.: Prog. Ser.* **1998**, *165*, 31−43.
(36) Ansari, A. A.; Abouhend, A. S.; Park, C. Effects of Seeding Density on Photogranulation and the Start-up of the Oxygenic Photogranule Process for Aeration-Free Wastewater Treatment. *Algal Res.* **2019**, *40*, 101495.
(37) Carreira, C.; Staal, M.; Middelboe, M.; Brussaard, C. P. D. Autofluorescence Imaging System to Discriminate and Quantify the Distribution of Benthic Cyanobacteria and Diatoms: Imaging Benthic Photoautotrophs. *Limnol. Oceanogr.: Methods* **2015**, *13* (4), No. e10016.
(38) APHA. *Standard Methods for the Examination of Water and Wastewater*; American Public Health Association: WA, 2012.
(39) Bennett, A.; Bogorad, L. Complementary Chromatic Adaptation in a Filamentous Blue-Green Alga. *J. Cell Biol.* **1973**, *58* (2), 419−435.
(40) Lawrenz, E.; Fedewa, E. J.; Richardson, T. L. Extraction Protocols for the Quantification of Phycobilins in Aqueous Phytoplankton Extracts. *J. Appl. Phycol.* **2011**, *23* (5), 865−871.
(41) Sobiechowska-Sasim, M.; Stoń-Egiert, J.; Kosakowska, A. Quantitative Analysis of Extracted Phycobilin Pigments in Cyanobacteria—an Assessment of Spectrophotometric and Spectrofluorometric Methods. *J. Appl. Phycol.* **2014**, *26* (5), 2065−2074.
(42) Zavřel, T.; Chmelík, D.; Sinetova, M. A.; Červený, J. Spectrophotometric Determination of Phycobiliprotein Content in

Cyanobacterium Synechocystis. *J. Vis. Exp.* **2018**, DOI: 10.3791/58076.
(43) Wezernak, C. T.; Gannon, J. J. Oxygen-Nitrogen Relationships in Autotrophic Nitrification. *Appl. Microbiol.* **1967**, *15* (5), 1211−1215.
(44) Adams, C. E.; Eckenfelder, W. W. Nitrification Design Approach for High Strength Ammonia Wastewaters. *J. Water Pollut. Control Fed.* **1977**, *49* (3), 413−421.
(45) Daigger, G. T. Oxygen and Carbon Requirements for Biological Nitrogen Removal Processes Accomplishing Nitrification, Nitritation, and Anammox. *Water Environ. Res.* **2014**, *86* (3), 204−209.
(46) Oxborough, K.; Baker, N. R. Resolving Chlorophyll a Fluorescence Images of Photosynthetic Efficiency into Photochemical and Non-Photochemical Components - Calculation of QP and Fv-/Fm-; without Measuring Fo-; *Photosynth. Res.* **1997**, *54* (2), 135−142.
(47) Hofstraat, J. W.; Peeters, J. C. H.; Snel, J. F. H.; Geel, C. Simple Determination of Photosynthetic Efficiency and Photoinhibition of Dunaliella Tertiolecta by Saturating Pulse Fluorescence Measurements. *Mar. Ecol.: Prog. Ser.* **1994**, *103*, 187−196.
(48) Platt, T.; Harrison, W. G.; Irwin, B.; Horne, E. P.; Gallegos, C. L. Photosynthesis and Photoadaptation of Marine Phytoplankton in the Arctic. *Deep-Sea Res., Part A* **1982**, *29* (10), 1159−1170.
(49) Giacometti, G. M.; Morosinotto, T. Photoinhibition and Photoprotection in Plants, Algae, and Cyanobacteria. In *Encyclopedia of Biological Chemistry*; Lennarz, W. J., Lane, M. D., Eds.; Academic Press: Waltham, 2013; pp 482−487. DOI: 10.1016/B978-0-12-378630-2.00229-2.
(50) Brightman, R.; Smith, W. Photosynthesis-Irradiance Relationships of Antarctic Phytoplankton during Austral Winter. *Mar. Ecol.: Prog. Ser.* **1989**, *53*, 143−151.
(51) Maxwell, K.; Johnson, G. N. Chlorophyll Fluorescence—a Practical Guide. *J. Exp. Bot.* **2000**, *51* (345), 659−668.
(52) Niyogi, K. K.; Truong, T. B. Evolution of Flexible Non-Photochemical Quenching Mechanisms That Regulate Light Harvesting in Oxygenic Photosynthesis. *Curr. Opin. Plant Biol.* **2013**, *16* (3), 307−314.
(53) Pocock, S. J. The Simplest Statistical Test: How to Check for a Difference between Treatments. *BMJ.* **2006**, *332* (7552), 1256−1258.
(54) Abouhend, A. S.; McNair, A.; Kuo-Dahab, W. C.; Watt, C.; Butler, C. S.; Milferstedt, K.; Hamelin, J.; Seo, J.; Gikonyo, G. J.; El-Moselhy, K. M.; Park, C. The Oxygenic Photogranule Process for Aeration-Free Wastewater Treatment. *Environ. Sci. Technol.* **2018**, *52* (6), 3503−3511.
(55) Palm, J. C.; Jenkins, D.; Parker, D. S. Relationship between Organic Loading, Dissolved Oxygen Concentration and Sludge Settleability in the Completely-Mixed Activated Sludge Process. *J. Water Pollut. Control Fed.* **1980**, *52* (10), 2484−2506.
(56) Figueroa, F. L. Relations between Electron Transport Rates Determined by Pulse Amplitude Modulated Chlorophyll Fluorescence and Oxygen Evolution in Macroalgae under Different Light Conditions. *Photosynth. Res.* **2003**, *75*, 259−275.
(57) González-Camejo, J.; Viruela, A.; Ruano, M. V.; Barat, R.; Seco, A.; Ferrer, J. Effect of Light Intensity, Light Duration and Photoperiods in the Performance of an Outdoor Photobioreactor for Urban Wastewater Treatment. *Algal Res.* **2019**, *40*, 101511.
(58) Babcock, G. T.; Barry, B. A.; Debus, R. J.; Hoganson, C. W.; Atamian, M.; McIntosh, L.; Sithole, I.; Yocum, C. F. Water Oxidation in Photosystem II: From Radical Chemistry to Multielectron Chemistry. *Biochemistry* **1989**, *28* (25), 9557−9565.
(59) Powles, S. B. Photoinhibition of Photosynthesis Induced by Visible Light. *Annu. Rev. Plant Physiol.* **1984**, *35* (1), 15−44.
(60) Morales, M.; Sánchez, L.; Revah, S. The Impact of Environmental Factors on Carbon Dioxide Fixation by Microalgae. *FEMS Microbiol. Lett.* **2018**, DOI: 10.1093/femsle/fnx262.
(61) Yen, H.-W.; Hu, I.-C.; Chen, C.-Y.; Chang, J.-S. Design of Photobioreactors for Algal Cultivation. In *Biofuels from Algae*; Elsevier, 2014; pp 23−45. DOI: 10.1016/B978-0-444-59558-4.00002-4.
(62) Holland, D. P.; Pantorno, A.; Orr, P. T.; Stojkovic, S.; Beardall, J. The Impacts of a High CO2 Environment on a Bicarbonate User: The Cyanobacterium Cylindrospermopsis Raciborskii. *Water Res.* **2012**, *46* (5), 1430−1437.
(63) Tang, K.-H.; Tang, Y. J.; Blankenship, R. E. Carbon Metabolic Pathways in Phototrophic Bacteria and Their Broader Evolutionary Implications. *Front. Microbiol.* **2011**, DOI: 10.3389/fmicb.2011.00165.
(64) Stauch-White, K.; Srinivasan, V. N.; Camilla Kuo-Dahab, W.; Park, C.; Butler, C. S. The Role of Inorganic Nitrogen in Successful Formation of Granular Biofilms for Wastewater Treatment That Support Cyanobacteria and Bacteria. *AMB Express* **2017**, DOI: 10.1186/s13568-017-0444-8.
(65) Subashchandrabose, S. R.; Ramakrishnan, B.; Megharaj, M.; Venkateswarlu, K.; Naidu, R. Mixotrophic Cyanobacteria and Microalgae as Distinctive Biological Agents for Organic Pollutant Degradation. *Environ. Int.* **2013**, *51*, 59−72.
(66) Wan, N.; Abernathy, M.; Tang, J. K.-H.; Tang, Y. J.; You, L. Cyanobacterial Photo-Driven Mixotrophic Metabolism and Its Advantages for Biosynthesis. *Front. Chem. Sci. Eng.* **2015**, *9* (3), 308−316.
(67) Ali, A.; Ammar, S.; Farid, H.; Lefkir, A.; Sayah, H. E.; Boubekeur, N. Just Suspended Speed for Solid Particle Transport in TorusReactor. In *New Trends in Urban Drainage Modelling*; Mannina, G., Ed.; Springer International Publishing: Cham, 2019; pp 879−885. DOI: 10.1007/978-3-319-99867-1_152.
(68) The influence of particles on suspension rheology. *Anton Paar Wiki*. https://wiki.anton-paar.com/en/the-influence-of-particles-on-suspension-rheology/ (accessed 2019-05-26).
(69) Kawase, Y.; Moo-Young, M. Mixing Time in Bioreactors. *J. Chem. Technol. Biotechnol.* **1989**, *44* (1), 63−75.
(70) *Handbook of Industrial Mixing: Science and Practice*; Paul, E. L., Atiemo-Obeng, V. A., Kresta, S. M., Eds.; Wiley-Interscience: Hoboken, NJ, 2004.
(71) da C. A. Alves, P. L.; Magalhães, A. C. N.; Barja, P. R. The Phenomenon of Photoinhibition of Photosynthesis and Its Importance in Reforestation. *Bot. Rev.* **2002**, *68* (2), 193−208.
(72) Han, B.-P.; Virtanen, M.; Koponen, J.; Straškraba, M. Effect of Photoinhibition on Algal Photosynthesis: A Dynamic Model. *J. Plankton Res.* **2000**, *22* (5), 865−885.
(73) Takahashi, S.; Badger, M. R. Photoprotection in Plants: A New Light on Photosystem II Damage. *Trends Plant Sci.* **2011**, *16* (1), 53−60.
(74) Gray, G. R.; Hope, B. J.; Qin, X.; Taylor, B. G.; Whitehead, C. L. The Characterization of Photoinhibition and Recovery during Cold Acclimation in Arabidopsis Thaliana Using Chlorophyll Fluorescence Imaging. *Physiol. Plant.* **2003**, *119* (3), 365−375.